Detailed Chemical Kinetic Modeling of Cyclohexane Oxidation†

Emma J. Silke,*,‡ William J. Pitz,‡ Charles K. Westbrook,‡ and Marc Ribaucour§

Lawrence Livermore National Laboratory, Livermore, California 94550, and PhysicoChimie des Processus de la Combustion, UMR CNRS/8522, Université des Sciences et Technologies de Lille, Bâtiment C11, 59655 Villeneuve d'Ascq, France

Received: November 15, 2006; In Final Form: January 12, 2007

A detailed chemical kinetic mechanism has been developed and used to study the oxidation of cyclohexane at both low and high temperatures. Rules for reaction rate constants are developed for the low-temperature combustion of cyclohexane. These rules can be used for in chemical kinetic mechanisms for other cycloalkanes. Because cyclohexane produces only one type of cyclohexyl radical, much of the low-temperature chemistry of cyclohexane is described in terms of one potential energy diagram showing the reaction of cyclohexyl radical with O_2 through five-, six-, and seven-membered-ring transition states. The direct elimination of cyclohexene and HO_2 from RO_2 is included in the treatment using a modified rate constant of Cavallotti et al. (*Proc. Combust. Inst.* 2007, *31*, 201). Published and unpublished data from the Lille rapid compression machine, as well as jet-stirred reactor data, are used to validate the mechanism. The effect of heat loss is included in the simulations, an improvement on previous studies on cyclohexane. Calculations indicated that the production of 1,2-epoxycyclohexane observed in the experiments cannot be simulated according to the current understanding of low-temperature chemistry. Possible "alternative" H-atom isomerizations leading to different products from the parent O_2QOOH radical were included in the low-temperature chemical kinetic mechanism and were found to play a significant role.

Introduction

Cycloalkanes are an important chemical class of hydrocarbons found in diesel, jet, and gasoline fuels. As the price of crude oil rises, Canada's oil-sand reserves are fast becoming an attractive source of synthetic crude oil. Canada's oil-sand reserves are second only to Saudi Arabia's proven oil reserves.[1] With the emergence of oil-sand-derived fuels, their role will become more important in future transportation fuels. Diesel fuel derived from oil sands is expected to have a higher cycloalkane content, which will affect the ignition quality of the fuel and soot emissions from its use in diesel-fueled cars and trucks. As a result, the effect of the composition of these oil-sand-derived fuels on combustion in vehicles is of immediate interest. In addition to being expected to be present in large amounts in diesel fuel derived from oil sands, cycloalkanes are a significant component of conventional diesel fuel (up to approximately 35%), jet fuels (~20%), and gasoline (~10%).[2,3] Cycloalkanes can raise soot emission levels because they are known to dehydrogenate and produce aromatics, which can lead to the production of polycyclic aromatics that are thought to be inception sites for soot growth.[4−6] As such, validated chemical kinetic mechanisms for cycloalkanes are needed to treat the oxidation of cycloalkanes under engine conditions.

Diesel, gasoline, jet, and oil-sand-derived fuels are complex mixtures of hundreds to thousands of hydrocarbons. It is not computationally feasible to include all of these components in a model with detailed chemistry. Therefore, chemical kinetic models with a limited number of components (called surrogate fuel models) are presently used to treat these practical fuels.

Generally, one or two components from each chemical class (*n*-alkanes, isoalkanes, cycloalkanes, alkenes, and aromatics) are selected to represent these chemical classes in a surrogate fuel. Because of the high proportion of cycloalkanes in practical fuels, detailed mechanisms for cycloalkanes are needed to simulate this chemical class. These mechanisms need to be valid under conditions found in internal combustion engines so that, when they are inserted into surrogate fuel models, they can be used to simulate combustion in spark ignition, homogeneous charge compression ignition (HCCI), diesel, and jet engines. Such surrogate fuel models are valuable in optimizing the design and performance of these engines and minimizing their pollutant emissions.[7]

To begin the development of chemical kinetic models for cycloalkanes, we started with cyclohexane, the simplest of cycloalkanes. We chose cyclohexane because considerably more experimental data are available for cyclohexane than for other cycloalkanes. Also, because of its simplicity, cyclohexane is a good starting case for the development of reaction rate rules for cycloalkanes. These reaction rate rules can be used later in the development of mechanisms for larger cycloalkanes, which are more representative of components present in diesel and jet fuels. In this article, we focus on the low- and intermediate-temperature chemistry of cyclohexane because the prediction of this chemistry is critical for correct simulation of ignition in HCCI and diesel engines.

Previous Cyclohexane Studies

Many chemical kinetic studies on the oxidation of *n*-alkanes and branched alkanes have been performed in recent years.[8] There are considerably fewer comparable studies on the kinetics of cycloalkanes in general and cyclohexane in particular, but these studies cover a rather wide range of experimental
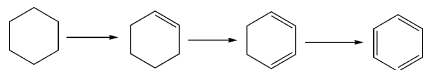
Figure 1. Formation of benzene from cyclohexane via cyclohexene and cyclohexa-1,3-diene.

conditions. Cyclohexane kinetics have been examined experimentally in shock tubes,[9,10] in a rapid compression machine (RCM),[11] in a jet-stirred reactor (JSR),[12,13] in a plug-flow reactor,[14] in closed reactors,[5,6,15−19] and in laminar premixed[4,20] and non-premixed[21] flames. General features of cyclohexane oxidation, according to these works, are that cyclohexane oxidation at high temperatures can take place through several distinct reaction pathways, including unimolecular decomposition of cyclohexane leading to linear products and H-atom abstraction leading to both dehydrogenation and formation of benzene and β-scission reactions that break the cyclic ring. The relative importance of each of these pathways varies widely from one oxidation environment to another.

At lower temperatures, addition of molecular oxygen to cyclohexyl radicals is generally observed, followed by internal H-atom-transfer reactions and other pathways leading to a negative-temperature-coefficient (NTC) region similar to those observed for many *n*-alkane and isoalkane hydrocarbon fuels. The only available experimental data on cyclohexane ignition across the NTC region from 700 to 850 K were reported by Lemaire et al.,[11] and these data have been used by all subsequent kinetic modeling programs to validate the low-temperature portions of the proposed reaction mechanisms.

Recently, kinetic modeling studies of cyclohexane oxidation have begun to appear, with both high-temperature[9,10,13] and combined high- and low-temperature[22−24] reaction mechanisms being developed.

Several major issues were identified in past publications that are still not completely resolved, and one goal of the present work is to address these issues. Dehydrogenation of cyclohexane to produce benzene is a potentially important pathway leading to soot formation. It is distinct from the more familiar routes that require aromatic ring formation by reactions involving C_3H_3, C_4H_5, and similar smaller species.[25] The cyclohexa-1,3-diene and benzene products of this reaction pathway have been observed in some of the cyclohexane studies,[4,5,11,12,26] whereas in others,[21] they have not.

There are two interesting questions regarding possible distinctions between the classes of reactions in cyclic alkanes and the same classes of reactions in *n*-alkane and isoalkane species. The major pathway for consumption of cyclohexane is H-atom abstraction by radicals, especially H, OH, and HO_2. The C−H bonds in cyclohexane are quite similar to secondary C−H bonds in *n*-alkanes such as *n*-heptane, so some kinetics researchers have assumed that the rates of H-atom abstraction in cyclohexane should be very close to the rates of secondary H-atom abstraction in *n*-heptane. The limits of such assumptions should be assessed.

In addition, in the low-temperature regime, the most sensitive reactions determining the rate of autoignition in acyclic alkanes such as *n*-heptane[27] or isooctane[28] involve internal H-atom transfers in RO_2 and O_2QOOH species. The same types of species are observed in low-temperature ignition of cyclohexane, including cyclohexyl−O_2 and O_2QOOH species, but an important question is how to estimate the rates of these reactions. In a recent kinetic modeling study of methylcyclohexane autoignition by Pitz et al.,[29] it was found that the presence of the cyclic ring contributes to the activation energy barriers for these isomerization reactions, and the recent study of Buda et al.[22] reached the same conclusion for cyclohexane.
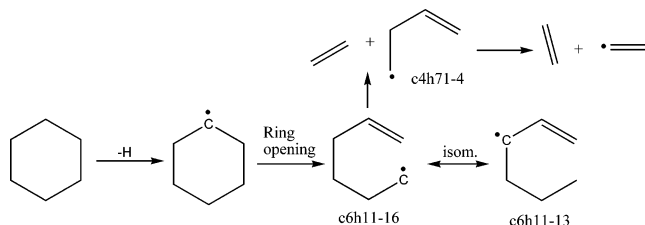

Figure 2. Example of a ring-opening reaction, followed by alkyl radical isomerization.

A goal of the present work is to determine the similarities and differences in the correction terms between cyclic and acyclic isomerization reactions in order to establish a formula for future mechanism development for other cyclic hydrocarbon species.

Chemical Kinetic Mechanism

The kinetic mechanism used in this study was developed by adding all of the species and reactions relating to the low- and high-temperature chemistry of cyclohexane (CHX) to the previously developed and validated mechanisms for C_1-C_6[28] and was constructed as a hierarchy of sequential hydrocarbon−oxygen systems. Submechanisms for toluene, benzene, and cyclopentadiene and the most recently published mechanism for methylcyclohexane were also included.[29,30] Reaction paths for cyclohexane were delineated, and reaction rate constants for both low- and high-temperature oxidation of cyclohexane were estimated or assembled using data in the literature. The THERM program of Ritter and Bozzelli,[31,32] which uses the group-additivity method of Benson,[33] was used to evaluate thermodynamic properties for all chemical species, including stable molecules and relevant radicals. The chemical kinetic mechanism and thermochemical property files are available as Supporting Information.

The mechanism development in the current work concerned both high- and low-temperature chemistry for cyclohexane, which includes all of the reactions known to be pertinent for these temperature regimes. At high temperatures, the reactions known to be important include unimolecular fuel decomposition, H-atom abstraction, alkyl radical decomposition, and addition to O_2, as well as isomerization reactions. Indeed, the well-documented formation of benzene via the dehydrogenation of cyclohexane is included and noted in the later discussion. The dehydrogenation of cyclohexane forms cyclohexene, which in turn can form cyclohexa-1,3-diene (and, to a lesser extent, cyclohexa-1,4-diene) and then benzene (Figure 1). For fuel-rich mixtures, benzene can lead to polycyclic aromatic hydrocarbons that are currently thought to act as sites for soot inception. Therefore, properly predicting the amount of benzene formed is an important step toward prediction of soot formation from cyclohexane.

At lower temperatures, the dominant reaction path for cyclohexane is H-atom abstraction from the parent fuel molecule by OH, HO_2, and other radicals, followed by successive additions of oxygen leading to chain-branching pathways, through the well-established low-temperature reaction scheme.[27] This scheme follows the addition of the cyclohexyl radicals (R) to O_2 and subsequent reactions, including cyclohexylperoxy (RO_2) isomerization to hydroperoxycyclohexyl radicals (QOOH) and decomposition of QOOH to cyclic ethers as well as other products.

Hydroperoxycyclohexyl radicals (QOOH) can also add to O_2 resulting in O_2QOOH, which can then isomerize to give carbonylhydroperoxide (or "ketohydroperoxide") species and

Chemical Kinetic Modeling of Cyclohexane Oxidation

J. Phys. Chem. A, Vol. 111, No. 19, 2007 **3763**
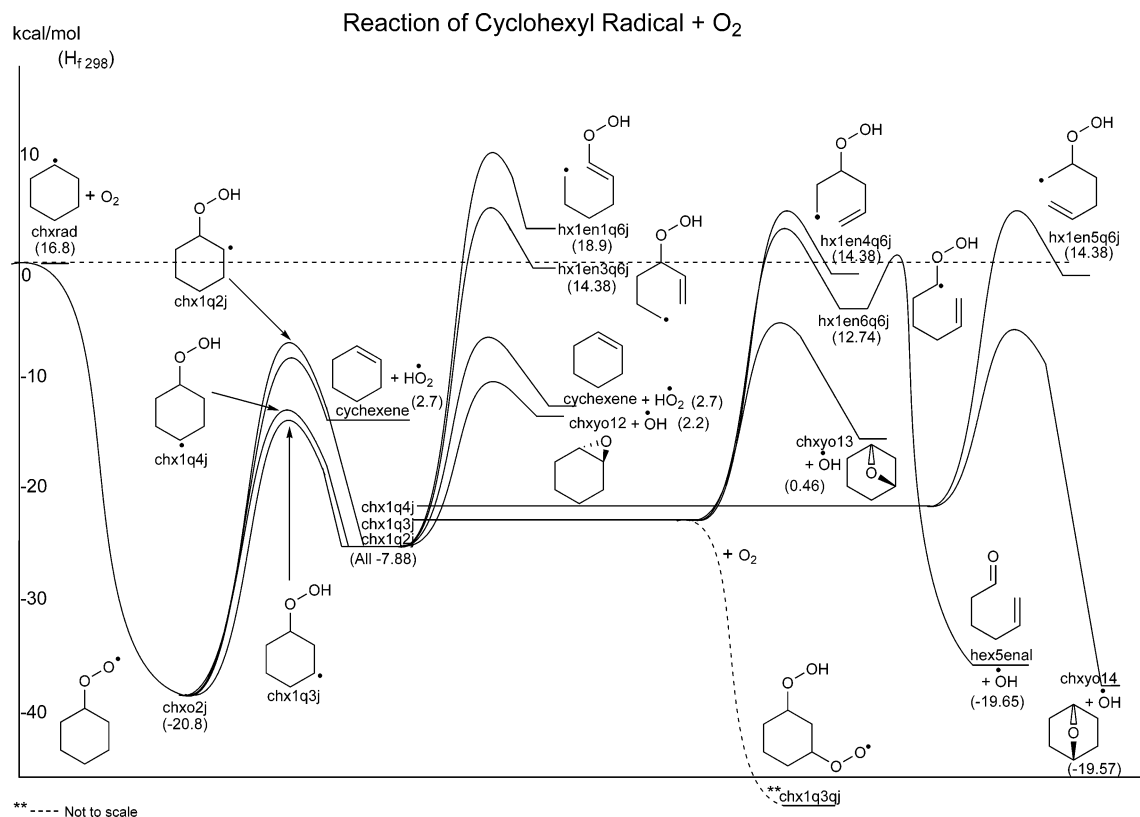

Figure 3. Potential energy diagram for the reaction of cyclohexyl radical (R) with O_2, based on thermodynamic properties determined in this work.

a hydroxyl radical. This carbonylhydroperoxide can decompose and yield a second hydroxyl radical.

In the next section, we discuss specific classes of elementary reactions and their rate constant determination. We discuss the most important reactions consuming the fuel and the subsequent reaction pathways.

Reaction Rate Constant Determination

In the following section, the rate rules employed for initiation reactions (including unimolecular fuel decomposition and molecular elimination reactions), H-atom abstraction from the fuel, alkyl radical decomposition, alkyl radical isomerization, alkyl radical consumption, and the subsequent reaction classes pertinent to the low-temperature regime are discussed.

Unimolecular fuel decomposition for cyclohexane can initiate through bond homolysis on the six-membered ring, which leads to the formation of a C_6H_{12} diradical. The rate constant for this reaction class was specified by a reverse recombination rate constant of $1.0 \times 10^8 T^{0.86}$. This rate constant is analogous to the rate constant employed in the methylcyclohexane mechanism of Orme et al.[34] for carbon radical−radical recombination, resulting in the formation of a ring structure. Our rate constant is approximately 1.4 times higher than that used by Sirjean et al.[9] for the unimolecular initiation reaction of cyclohexane resulting in a diradical.

Molecular elimination reactions for cyclohexane were included such that the parent fuel could eliminate either two propene molecules or three ethene molecules. The rate constants for both of these reactions were assumed to be the same as that of 1-hexene eliminating two propene molecules, which is given by the Tsang[35] rate constant expression of $4.0 \times 10^{12} \exp(-57400 \text{ cal}/RT)$ cm^3 mol^{-1} s^{-1}.

In cyclohexane, all of the sites available for *hydrogen-atom abstraction* are equivalent, as abstraction is always from a secondary site embedded in a ring structure. The environment of such a ring-bound secondary H-atom is somewhat different from that of a normal secondary H-atom. For abstraction by H, O, OH, CH_3, CH_3O, C_2H_3, and C_2H_5 of secondary C−H bonds, we assumed the rate constant to be similar to that of a normal secondary H-atom and employed the recommended rates of Curran et al.[28] For H-atom abstraction by HO_2, we used a cyclohexane-specific rate, determined by Handford-Styring and Walker[6] in their study of H-atom abstraction by HO_2 from secondary C−H sites in cyclohexane. The rate employed for H-atom abstraction by HO_2 was $1.12 \times 10^5 T^{2.5} \exp(-14147 \text{ cal}/RT)$ cm^3 mol^{-1} s^{-1}. For abstraction by CH_3O_2 and cycloalkylperoxy radical, we assumed that the rate constant was the same as that for the analogous reaction of HO_2 abstraction of a secondary H-atom, as reported by Scott and Walker,[36] such that the rate expression used for both of these reactions was $1.47 \times 10^5 T^{2.5} \exp(-14863 \text{ cal}/RT)$ cm^3 mol^{-1} s^{-1}.

Rate constants for *alkyl radical decomposition* were specified in the reverse, exothermic direction, that is, for the addition of an alkyl radical to an alkene. Rate constants for the addition of radicals to a double bond depend on a number of factors, namely, the type of radical undergoing to addition and the nature of the site to which it is adding, i.e., an internal or terminal C atom. The rate expressions used were taken from the recent work of Curran,[37] who evaluated rate constants for C_1−C_4 alkyl and alkoxyl radical decomposition. In our rate constant estimations, we considered the type (primary, secondary, or tertiary) and size of alkyl radical, as well as the type of site (internal or terminal) on the alkene to which the radical was adding.

In the case of *ring-opening reactions*, for species with radical sites on the C_6 ring, rate constants were estimated in the reverse direction. An example of a ring-opening reaction is illustrated as the "ring-opening" step in Figure 2. The reverse of the ring-opening step is a methyl radical adding to the terminal group

3764 *J. Phys. Chem. A, Vol. 111, No. 19, 2007*

Silke et al.

of an olefin, forming a cyclic structure. Rate constants for such reactions were taken from Matheu et al.,[38] who reviewed and estimated high-pressure rate constants for these reactions. For example, the rate constant used for the endo 1,6-intramolecular addition in Figure 2 was $1.00 \times 10^8 \, T^{0.86} \exp(-5900 \text{ cal}/RT)$ cm^3 mol^{-1} s^{-1}.

The rate constants used for *alkyl radical isomerization* in this study were taken from Matheu et al.,[38] who used high-level quantum calculations (B3LYP-ccpVDZ) for such isomerizations or "H-shifts". For example, the isomerization in Figure 2 illustrates a 1,4 H-shift (five-membered transition state) of a primary radical shifting to an allylic radical site with a rate expression of $3.67 \times 10^{12} \, T^{-0.6} \exp(-15300 \text{ cal}/RT)$ cm^3 mol^{-1} s^{-1}.

Low-Temperature Chemistry Scheme

Reaction rate constants for the low-temperature oxidation of cyclohexane were developed based on those previously developed for methylcyclohexane.[29] In particular, Pitz et al. reported that the use of noncyclic alkylperoxy isomerization rates led to a dominance of seven-membered-ring isomerizations, which lead to chain-propagation channels, as opposed to the chain-branching paths associated with six-membered rings, and attributed this dominance to the lack of low-temperature chain branching for methylcyclohexane. They subsequently showed that the use of cyclo-specific rate rules was necessary to simulate the experimental data for cyclic systems, and such specifics will be discussed here according to reaction class.

The first step in the low-temperature chemistry scheme is illustrated in Figure 3, where the potential energy diagram for the addition of molecular oxygen to the cyclohexyl radical is depicted. Conveniently, cyclohexane has only one isomer. Because such an addition of molecular oxygen is dependent on the nature of the radical site where the addition is to occur, the rate constant applied was based on an analogy to that used in a methylcyclohexane study[29] for addition to a secondary alkyl radical, 3.0×10^{12} cm^3 mol^{-1} s^{-1}.

The next step in the low-temperature reaction scheme is *alkylperoxy isomerization*. In this work, we employed the rate constants used in the methylcyclohexane study of Pitz et al.[29] They used the noncyclic alkylperoxy isomerization rate recommendations of Curran et al.[28] (Table 1) and corrected them for the cyclohexyl case. The corrections they employed were taken from the *n*-alkane and specific cyclohexane rate constants of Walker and co-workers,[5,6] where kinetic data for H-atom transfer in cyclohexylperoxy radical (CHXO$_2$) were compared to kinetic data Walker and co-workers had previously published for noncyclic alkylperoxy radicals.[39] The details of the modification are shown in Table 1, where the kinetic data in use in this study are reported.

Recent studies, including that of Carstensen et al.,[41] on *n*-alkanes such as ethane and propane have highlighted the importance of the direct elimination of olefin and a hydroperoxyl from RO$_2$. We included the direct elimination pathway in our cyclohexane mechanism and found ignition delay times to be highly sensitive to the rate expression in use for this reaction. We employed the rate constant computed by Cavallotti et al.,[23] where we have reduced the *A* factor by a factor of 2 such that the expression in use is $3.85 \times 10^{12} \exp(-29000 \text{ cal}/RT)$ cm^3 mol^{-1} s^{-1}.

In addition, we employed slightly modified versions of the Cavallotti recommendations for the formation of cyclic ether and a hydroxyl radical from QOOH radicals (Table 2). These modifications of the rate constants were necessary for agreement

TABLE 1: Rate Constant Expressions for Cyclic Alkylperoxy (RO$_2$) isomerization Used in Present Study, Including Illustration of Rate Adjustment[a]

ring size in transition state	A	n	E$_a$	rate at 750 K
Curran et al.:[28] Noncyclic Alkylperoxy				
5	1.0×10^{11}	0	26850	6.0×10^3
6	1.25×10^{10}	0	20850	4.2×10^4
7	1.56×10^9	0	19050	8.8×10^3
Handford-Styring and Walker:[6] Cyclohexylperoxy				
5 (1,4s)	8.71×10^{11}	0	32433.1	3.1×10^2
6 (1,5s)	6.46×10^{11}	0	29517.2	1.6×10^3
7 (1,6s)	7.59×10^{10}	0	26816.4	1.2×10^3
Walker and Morley:[39] Noncyclic Alkylperoxy				
5	1.41×10^{12}	0	31787.8	7.7×10^2
6	1.74×10^{11}	0	26290.6	3.8×10^3
7	2.19×10^{10}	0	21510.5	1.2×10^4
	A_{cyclo}/A_{normal}	$E_{a,cyclo} - E_{a,normal}$	k_{cyclo}/k_{normal}	
5	0.62	645.3	0.4	
6	3.72	3226.6	0.43	
7	3.47	5305.9	0.1	
Curran et al.:[28] Alkylperoxy Rate Modified for Cyclic RO2 System (Used in This Work)				
5	$4.94 \times 10^{11 \, b}$	0	31000^c	4.6×10^2
6	$1.86 \times 10^{11 \, d}$	0	24076.6^e	1.8×10^4
7	1.08×10^{10}	0	24355.9	8.6×10^2

^{a} Units of cm^3 mol s cal; all secondary C−H sites; rate at 750 K accounts for degeneracy. ^{b} $A_{Curran} \times (A_{cyclo}/A_{normal}) \times$ degeneracy $\times 2$ (where the latter factor is for experimental agreement). ^{c} $E_a = E_a$ for HO$_2$ elimination of DeSain et al.[40] + 2 kcal. ^{d} $A_{Curran} \times (A_{cyclo}/A_{normal}) \times$ degeneracy. ^{e} $E_{a,Curran} + (E_{a,cyclo} - E_{a,normal})$.

TABLE 2: Rate Constant Parameters Used for Cyclic Ether Formation from QOOH Radicals (cm^3 mol s cal), Based on the Recommendations of Cavallotti et al.[23] and Modified as Described to Obtain Agreement with the Experimental Results

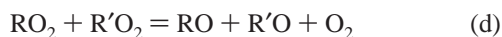| cyclic ether ring size	A	n	E$_a$
3	5.8×10^{12}	0	13400
4	1.4×10^{12}	0	20000
5	8.6×10^{12}	0	18500

with experiments, and a reduction in activation energy (E_a) from the Cavallotti value to those reported in Table 2 gave good agreement between the model and experiment for both 1,3- and 1,4-epoxycyclohexane. However, we were unable to match the experimental profile of 1,2-epoxycyclohexane (cyclic ether ring size of 3), even after increasing the *A* factor by a factor of 2 and reducing the activation barrier from 15.4 to 13.4 kcal mol^{-1}.

Hydroperoxycyclohexyl (QOOH) radicals, in which the radical site is located beta to the hydroperoxy group, can decompose to yield a conjugate olefin and HO$_2$ radical. The rate constant for this reaction was considered in the reverse direction, that is, the addition of a HO$_2$ radical to an olefinic site. We employed a rate constant expression of $8.0 \times 10^{10} \exp(-6000 \text{ cal}/RT)$ cm^3 mol^{-1} s^{-1}, similar to that used in the methylcyclohexane study of Pitz et al.[29]

Finally, QOOH radicals can undergo β-scission to form a multitude of products. For the hydroperoxycyclohexyl radicals this always involves an initial ring-opening step and subsequent β-scission to A radical and a stable intermediate species. We carefully considered the decomposition pathways of each QOOH radical in the mechanism.

Disproportionation reactions between radicals important at low temperature must be considered:

$$R + HO_2 = RO + OH \tag{a}$$

$$RO_2 + HO_2 = RO_2H + O_2 \qquad (b)$$

$$RO_2 + CH_3O_2 = RO + CH_3O + O_2 \qquad (c)$$

$$RO_2 + R'O_2 = RO + R'O + O_2 \qquad (d)$$

For each of these reactions, the rate rules proposed by Curran et al. in their work on isooctane were employed.[28]

For *ROOH dissociation*, the rate constant was considered in the reverse direction and was based on an analogy with the reaction of $CH_3O + OH$ by Tsang and Hampson,[42] so that we used 1.81×10^{13} cm^3 mol^{-1} s^{-1}. In the decomposition of RO, because it involves a cyclic system, there is an initial ring-opening step, followed by β-scission to form products. As per our regular rules, as described earlier, we considered this ring-opening step in the reverse direction and used 1.00×10^8 $T^{0.86}$ $exp(-5900$ $cal/RT)$ cm^3 mol^{-1} s^{-1}, the Matheu et al.[38] recommendation for 1,6-intramolecular addition (endo).

For the *addition of QOOH to O_2*, the rate expressions used were identical to those for cyclohexyl addition to O_2 discussed earlier in this article. The resulting species, O_2QOOH, can isomerize to form a carbonylhydroperoxide and a hydroxyl radical. The rate constant for this process, as well as for other isomerizations via an internal hydrogen atom, which result in what we term "alternative" O_2QOOH, are analogous to those for RO_2 isomerizing to QOOH. For *O_2QOOH isomerization* to carbonylhydroperoxide and a hydroxyl radical, the rate expressions used were based on the recommendations of Curran et al.[28] and are reported in Table 3. However, as with the noncyclic alkylperoxy isomerizations, the rate we used for this cyclic O_2-QOOH isomerization was modified to account for the ring structure. As with the previous studies of Curran et al. on *n*-heptane[27] and isooctane,[28] the activation energy was reduced by 3 kcal mol^{-1} because the hydrogen atom being abstracted is bound to a carbon atom that is bound to a hydroperoxy group and should, in turn, be more easily removed.

Alternative O_2QOOH. In the previous studies on *n*-heptane and isooctane by Curran et al.,[27,28] only one internal H-atom isomerization step for O_2QOOH was considered: the hydrogen atom abstracted was the one bonded to the carbon atom having the $-OOH$ functional group, such that the products were always a stable carbonylhydroperoxide species and a hydroxyl radical, as shown in Figure 4.

At that time, Curran et al. also argued that, for this particular H-atom isomerization, the C—H bond is weaker than that of a typical H-atom in a hydrocarbon species and, thus, the H-atom is more easily abstracted. However, ring-strain energies dictate that, in many instances, other conventional hydrogen atoms, which can form five-, six-, or seven-membered transitions states, are also available. Thus, O_2QOOH can also isomerize to form what we term alternative O_2QOOH, which can then ultimately decompose to a different set of products. Rate constant analysis for cyclohexane has shown that these alternative reactions are indeed competitive with the formation of the carbonylhydroperoxide and a hydroxyl radical. For this reason, the possibility of such alternative isomerizations occurring, leading to different products from the parent O_2QOOH, is permitted and included in this work on cyclohexane, along with the more conventional route forming carbonylhydroperoxide and a hydroxyl radical. An example of the alternative isomerization is illustrated in Figure 5, and Table 3 reports the reaction rates used in this work. Some interesting observations were made in relation to the sensitivity of including this additional low-temperature chemistry, and these are reported and discussed in detail in the next section of this article.
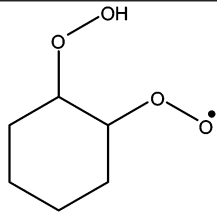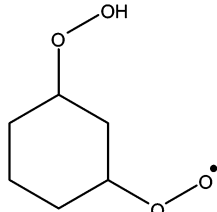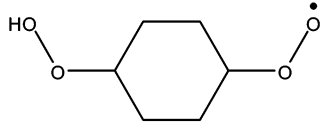
Results and Discussion

To validate the proposed mechanism, it was necessary to carry out simulations of experiments reported in the literature. In this section, we describe how the mechanism developed in this work was used to simulate experimental results obtained in a rapid compression machine (RCM)[11] and in a jet-stirred reactor (JSR).[12,13] The RCM study incorporated the range of temperatures at which negative-temperature-coefficient behavior is observed in the oxidation of cyclohexane.

Rapid Compression Machine. The experiments of Lemaire et al.[11] were conducted in a rapid compression machine at a compression ratio of 9.3, covering the compressed-gas temperature range of 650−900 K and varying compressed-gas pressures. In addition, many combustion products were identified in their work, including bicyclic epoxides, cyclic ketones, unsaturated aliphatic aldehydes, and conjugated alkenes. Stoichiometric mixtures of fuel and "air" were used, with the diluent consisting of various mixtures of $N_2/Ar/CO_2$, which enabled the heat capacity of the mixture, and thus the compressed-gas temperature, to be varied. The pressure at top dead center (TDC), which is dependent on both the initial gas pressure used and the combination of the inert substances making up the diluent gas, was varied between 6.9 and 13.8 atm. We simulated their experimental results assuming a homogeneous reactor, using SENKIN[43] and AURORA[44] codes in the Chemkin suite of programs. The temperature and species concentrations were assumed to be uniform across the combustion chamber. In the first series of calculations, constant-volume adiabatic calculations were performed at the conditions at the end of compression. As will be seen later, these calculations were quite accurate. The effect of including the compression stroke was small, and the effect of heat loss was important only for the lowest temperatures.

Lemaire et al. reported their experimental data for the ranges of compressed-gas pressures 7−9 and 11−14 atm, and we assumed average pressures of 8 and 12.5 atm for our simulations, a diluent gas of N_2 only, and compressed-gas temperatures within the range of 650−900 K as the initial conditions for constant-volume calculations. The effect of including the actual diluent composition on the computed ignition delay time was very small because the compressed-gas temperature was specified. The ignition delay time in the model calculations was defined as the time from the end of compression to the maximum rate of pressure rise due to ignition. The cool flame delay time was taken as the time from the end of compression to the time where a slight pressure rise due to the first-stage ignition event was observed. The results shown in Figures 6 and 7 illustrate the model-predicted ignition delay times for the adiabatic, constant-volume calculations versus the RCM experimental data of Lemaire et al.[11]

The model-predicted cool flame and total ignition delay times were found to be within reasonable agreement of these experimental data. The trend of decreasing ignition delay time with increasing pressure agrees well between the experiments and the model for the entire temperature range in question. Note that the scale for ignition delay time is reduced at the higher pressure used in Figure 7. Prominent NTC behavior was observed for both pressure studies conducted. The model reproduced two-stage ignition for both pressures investigated and up to compressed-gas temperatures of ∼770 K. Figure 8 illustrates the model-predicted cool flame and total ignition delay times, as well as the transition into the NTC region where the ignition delay times are seen to elongate. The two-stage ignition, or cool flame, is observed as a small "shoulder" in the pressure−

TABLE 3: Rate Constant Parameters Used for O₂QOOH Isomerizations, Including Illustration of Rate Adjustment^{a,b}

Ring Size in transition State	A	n	Ea	Rate at 750 K	
Curran *et al.* Alkylperoxy rate modified for cyclic O₂QOOH to Carbonyl-hydroperoxide system – in use in this work					
5	6.17e+10	0	24495.3	4.5e+3	
6	4.64e+10	0	21076.6	3.3e+4	
7	5.41e+9	0	21355.9	3.2e+3	
A$_{Curran}$ x ratio$_{(cyclo/normal)}$ x degeneracy(=1), Ea$_{Curran}$ + difference$_{(cyclo/normal)}$ – 3 kcal for weak C-H					
Curran *et al.* Alkylperoxy rate modified for cyclic O₂QOOH to 'alternative' O₂QOOH system – *in use in this work*					
5	1.24e+11	0	24495.3	1.2e+3	
6	1.86e+11	0	21076.6	1.8e+4	
7	1.08e+10	0	21355.9	8.6e+2	
5	2.48e+11	0	24495.3	2.4e+3	
6	9.3e+10	0	21076.6	8.95e+3	
7	1.08e+10	0	21355.9	8.6e+2	
5	2.48e+11	0	24495.3	2.4e+3	
6	1.86e+11	0	21076.6	1.8e+4	
A$_{Curran}$ x ratio$_{(cyclo/normal)}$ x degeneracy, Ea$_{Curran}$ + difference$_{(cyclo/normal)}$ – 3 kcal* (*reduction for agreement with experiments)					

^{a} Units of cm^3 mol s cal; all secondary C−H sites; rate at 750 K accounts for degeneracy. ^{b} $A_{Curran} \times (A_{cyclo}/A_{normal}) \times$ degeneracy; $E_{a,Curran} + (E_{a,cyclo} - E_{a,normal}) - 3$ kcal (where the latter reduction is necessary for agreement with experiments)
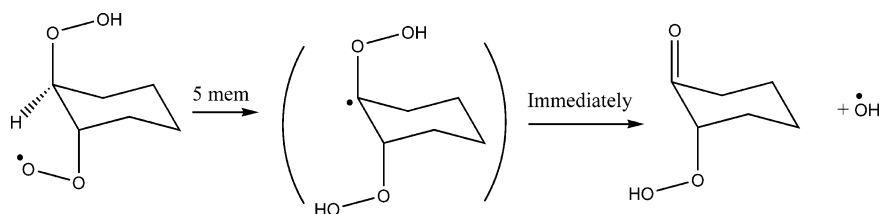
Figure 4. Example of the more conventional O₂QOOH isomerization leading to carbonylhydroperoxide + OH.

time profile. The experimental data show that two-stage ignition was recorded up to temperatures of approximately 800 K (see the temperature at which the open symbols terminate in Figures 6 and 7). However, two-stage ignition was not observed in the simulations at temperatures greater than 770 K (see the temperature at which the dotted line terminates in Figures 6 and 7).

Results from a simulation were compared to the experimental results at 727 K and 7.4 atm, where experimental species measurements were made for various bicyclic epoxides, cyclic ketones, unsaturated aliphatic aldehydes, and conjugated alkenes. In these experiments, selected reactive mixtures were allowed to expand into a sampling vessel and were analyzed qualitatively and quantitatively by gas chromatography and mass spectrom-

etry. Figures 9−14 illustrate the model predictions of various species that were measured experimentally in the RCM. The measured and predicted fuel concentration histories are shown in Figure 9. Results are shown as percent carbon in the fuel because this was the quantity measured in the experiments. The end of the first stage of ignition is seen clearly as an "elbow" in the computed fuel history. The model predicts that more fuel is consumed in the first-stage ignition than in the experiment. However, the location of the end of the first stage is not clearly seen in the fuel concentration measurements. (From Figure 6, the measured first-stage ignition time is about 25 ms.)

For the intermediate species, the model predicts most of the species that were recorded experimentally very well. Results for intermediate species are shown versus percent fuel consumed
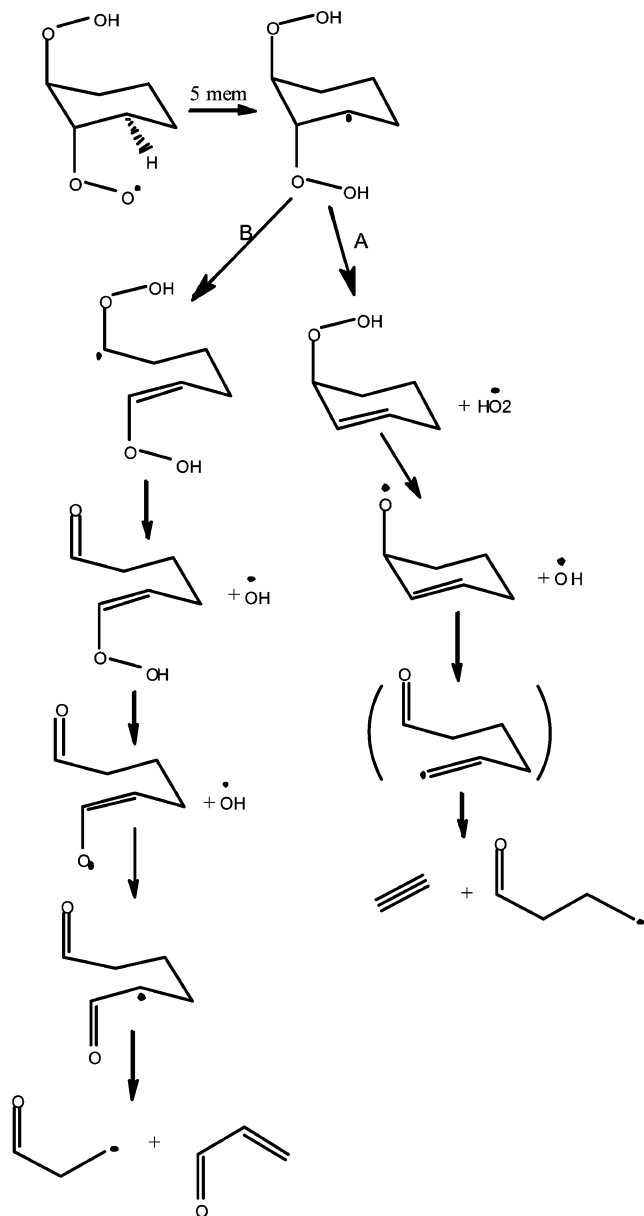
Figure 5. Example of the type of alternative O_2QOOH isomerizations permitted in this work. The example shows a five-membered transition state and two possible routes of decomposition.
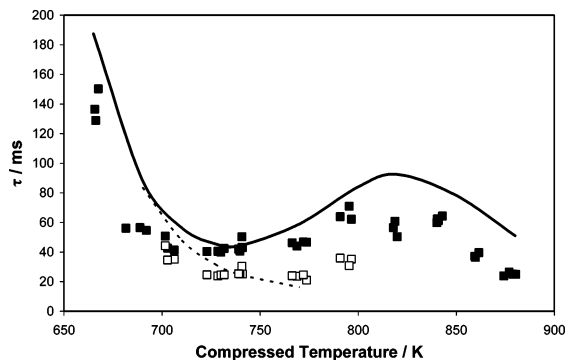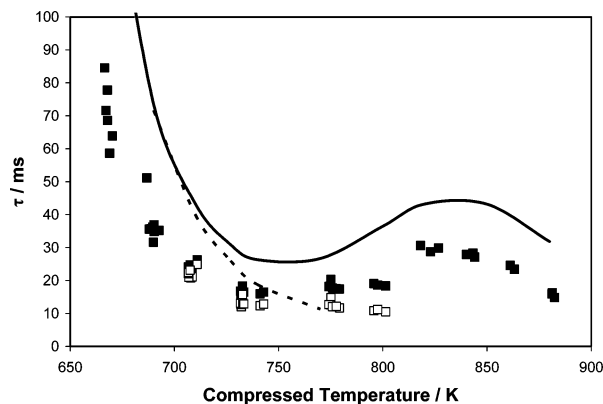

Figure 6. Experimental[11] (points) ignition delay times in the pressure range of 7−9 atm from a rapid compression machine investigation and model-predicted values (line) at 8 atm. Open symbols and dashed line correspond to cool flame delay times.

so that differences in the fuel concentration history are removed from the comparison. Our model predicts the formation of cyclohexa-1,3-diene and benzene products from the dehydro-

Figure 7. Experimental[11] (points) ignition delay times in the pressure range of 11−14 atm from a rapid compression machine investigation and model-predicted values (line) at 12.5 atm. Open symbols and dashed line correspond to cool flame delay times.
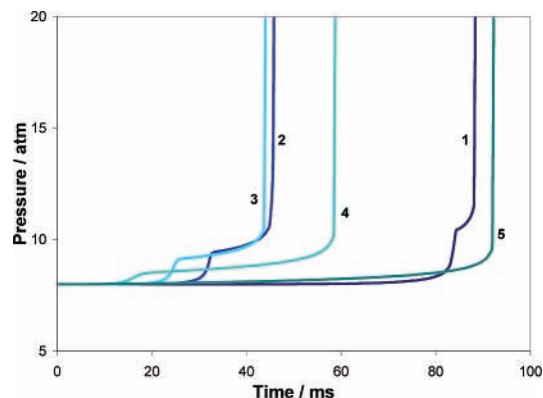
Figure 8. Model-predicted pressure−time profiles for rapid compression machine experiments, depicting NTC behavior and the appearance and disappearance of cool flame phenomena. Curves correspond to the following end-of-compression temperatures: (1) 690, (2) 727, (3) 740, (4) 770, and (5) 820 K. Time represents the time after the end of compression.
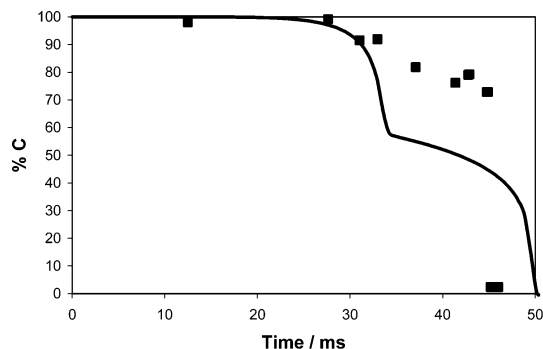

Figure 9. Comparison of experimental (points) and model-predicted (line) cyclohexane consumption profiles at 7.4 atm and 727 K in an RCM. Time represents the time after the end of compression.

genation reaction path of cyclohexane, in agreement with the observations of some cyclohexane studies.[4,5,11,12,26] However, benzene is underpredicted when compared to the experimentally measured quantity. Reaction flux analysis showed that most of the benzene produced in the simulation comes from the series of dehydrogenation reactions of cyclohexane, leading to benzene via cyclohexene and cyclohex-1,3-diene. In addition, our model underpredicts the amount of 1,2-epoxycyclohexane. Reaction flux analysis showed that the direct elimination pathway of RO_2 forming olefin + HO_2 dominated, reducing the amount of RO_2 available to isomerize to QOOH (chx1q2j) and form 1,2-epoxycyclohexane (chxyo12), as depicted in Figure 3.
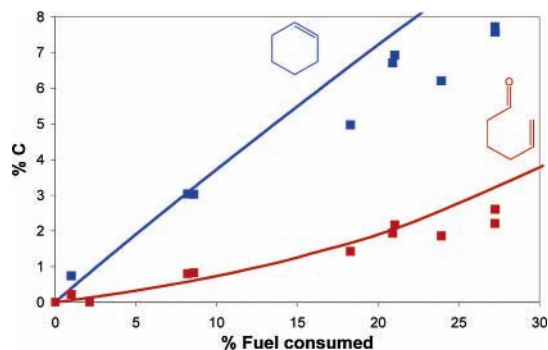
Figure 10. Species profiles in an RCM of cyclohexene (navy blue) and hex-5-enal (red): experimental, points; model, lines.
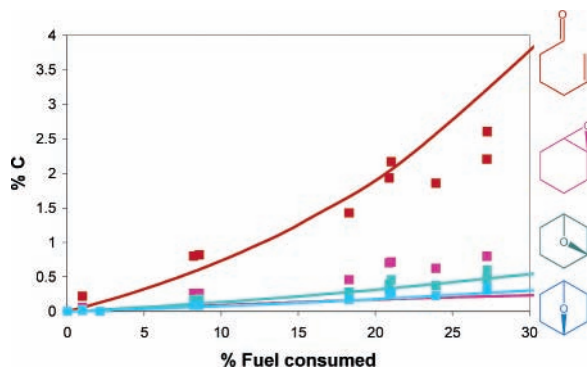

Figure 11. Species profiles in an RCM of hex-5-enal (red), 1,2-epoxycyclohexane (magenta), 1,3-epoxycyclohexane (green), and 1,4-epoxycyclohexane (blue): experimental, points; model, lines.
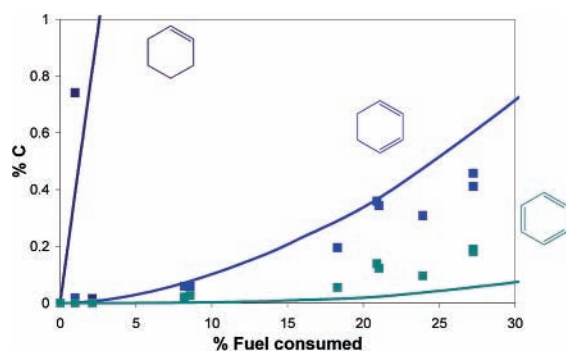

Figure 12. Species profiles of the soot precursors in an RCM (experimental, points; model, lines): cyclohexene (navy blue), cyclohexa-1,3-diene (blue), and benzene (green).
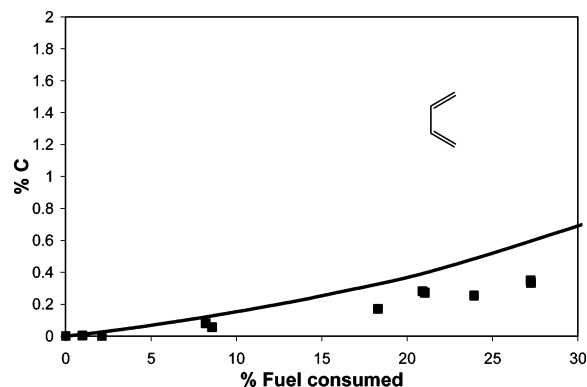

Figure 13. Species profile of 1,3-butadiene in an RCM (experimental, points; model, lines).
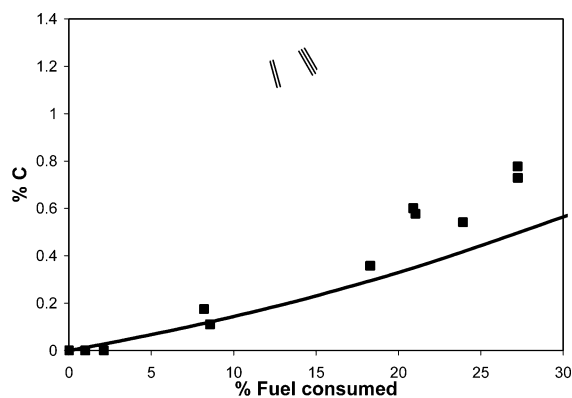
Figure 14. Species profile of ethene and ethyne (combined) in an RCM (experimental, points; model, lines).

When comparing computed and measured species concentrations, it is important to be aware of inhomogeneities in the temperature distribution in the combustion chamber and their effect on species concentrations. The species near the cold boundary layer experience lower temperatures than the hot core gases. For end-of-compression temperatures that lie in the NTC region, gases with a slightly lower temperature near the cold boundary layer will react faster than hotter core gases. Reactive species from these cooler gases could mix with and influence the reactivity of the hotter core gases. For compression temperatures outside the NTC region, the cooler gases near the cold boundary layer will react more slowly than the hotter core gases. This phenomenon will have an effect on the measured species concentrations and ignition delay times. This effect is somewhat compensated for in a zero-dimensional calculation, when an average heat loss is included.

Some Observations Using the Alternative O_2QOOH Reaction Class. In the previous studies on *n*-heptane and isooctane

by Curran et al.,[27,28] only one internal H-atom isomerization step for O_2QOOH was considered, such that the products were always a stable carbonylhydroperoxide species and a hydroxyl radical (Figure 4). This choice was based on analysis of reaction paths and C—H bond strength arguments. However, considerations of ring-strain energies dictate that, in many instances, other conventional hydrogen atoms that can form five-, six-, or seven-membered transitions states can also be abstracted. Thus, O_2QOOH can also isomerize to form what we term alternative O_2QOOH, which can then ultimately decompose to a different set of products. In a recent study, we completed the addition of such alternative O_2QOOH species and reactions to the *n*-heptane mechanism of Curran et al.[27,28] Silke et al.[45,46] found that, for some experimental parameters, the addition of this reaction class improved the performance of the *n*-heptane mechanism. However, for other experimental parameters, the *n*-heptane model deteriorated in its ability to match the experiments. Nevertheless, the recommendation was that this reaction class should be included.

Table 3 lists the rate constants that were used for the alternative O_2QOOH reaction class. During the course of this work, we found it necessary to reduce the activation energy used by 3 kcal mol^{-1} in order to obtain agreement with the experiments. Figure 15 displays a comparison of the simulations in which (A) the activation energy was estimated according to the reaction rate rules for analogous noncyclic alkylperoxy isomerizations, the definitions for which are listed in Table 2 for five-, six-, and seven-membered rings, and (B) the activation energies described for part A were reduced by 3 kcal mol^{-1}.

Sun and Bozzelli[47] recently performed ab initio and density functional calculations to evaluate reaction paths and kinetics for neopentyl oxidation. In their study, they reported an activation energy of approximately 23.8 kcal mol^{-1} for the RO_2-

Chemical Kinetic Modeling of Cyclohexane Oxidation

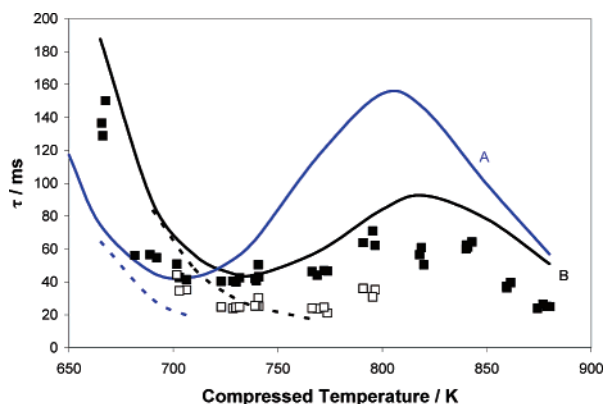*J. Phys. Chem. A, Vol. 111, No. 19, 2007* **3769**

Figure 15. Comparison of the performance of the mechanism used in this work when the activation energy for the alternative O_2QOOH reaction class is varied: Experimental (points) ignition delay times in the pressure range of 7−9 atm and model-predicted values (lines) at 8 atm. (A) Activation energy based on those of analogous cyclic alkylperoxy isomerizations and (B) activation energy as in A but with a reduction of 3 kcal mol^{-1}. Open symbols and dashed lines correspond to cool flame delay times.

to-QOOH isomerization. The subsequent second isomerization reactions, namely, O_2QOOH forming carbonylhydroperoxide or alternative O_2QOOH, had slightly lower activation energies, of 22.4 and 22.6 kcal mol^{-1}, respectively. We highlight the Sun and Bozzelli work as an interesting analogy to our own reaction rates: When we reduced the barrier of alternative O_2QOOH by 3 kcal mol^{-1}, we were using a value similar to the energy barrier for carbonylhydroperoxide formation, this being same trend of activation energies in use for O_2QOOH in the Sun and Bozzelli study.

First-order sensitivity analysis was carried out using the sensitivity analysis capability available in Aurora.[44] This sensitivity analysis examined the effect of a small change in the rate constant on the response parameter: the mole fraction of OH (hydroxyl radical). Three different temperatures were chosen to cover the temperature range of interest, namely, 650, 727, and 800 K, all of which were at an average pressure of 8 atm. Sensitivity analysis using the above criteria was carried for both versions of the mechanism, first, that in which the activation energy of the alternative O_2QOOH isomerization was based on analogous cyclic alkylperoxy isomerizations (Figure 16) and, second, that in which this activation energy was reduced by 3 kcal mol^{-1} (Figure 17).

The sensitivity analysis in Figure 16 shows that O_2QOOH proceeding via the carbonylhydroperoxide channel (labeled O_2-QOOH = keto + OH) contributes to the acceleration of the oxidation process. Indeed, isomerization to alternative O_2QOOH contributes to much the same extent (labeled O_2QOOH = altern. O_2QOOH). What is remarkable is that loss of a second OH from the carbonylhydroperoxide (labeled keto = product + OH) is accelerating in comparison to the decomposition of products formed via the alternative O_2QOOH isomerization (labeled O_2-QOOH altern. = product + OH), which is actually slowing at 650 K.

In Figure 17, the sensitivity analysis in which both O_2QOOH isomerization paths have the same activation energies, the formation of carbonylhydroperoxide accelerates the oxidation process in comparison to the formation of alternative O_2QOOH, which actually slows the oxidation process at 650 and 727 K. However, the alternative pathway accelerates the oxidation process (labeled O_2QOOH altern. = product + OH) more than loss of an OH group from the carbonylhydroperoxide (labeled keto = product + OH).
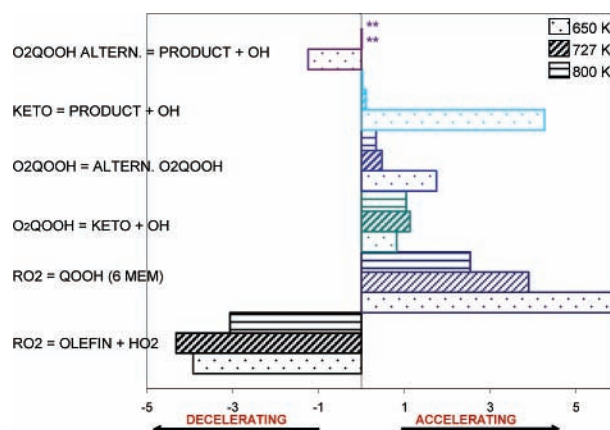

Figure 16. Sensitivity of the OH concentration to a change in reaction rate constant at three different end-of-compression temperatures. This version of the reaction mechanism is with the activation energy of alternative O_2QOOH paths 3 kcal mol^{-1} higher than that used for O_2-QOOH forming carbonylhydroperoxide. This reaction mechanism yielded reactivity profile A in Figure 15. (** indicates that all of the sensitivity values were negligible.)
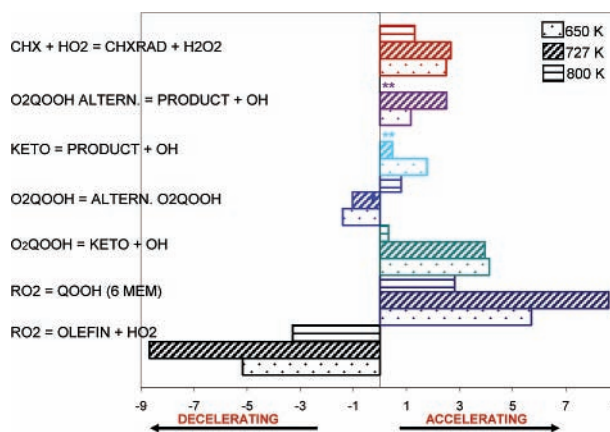

Figure 17. Sensitivity of the OH concentration to a change in reaction rate constant at three different end-of-compression temperatures. This version of the reaction mechanism is with the activation energy of alternative O_2QOOH paths being the same as that for used O_2QOOH forming carbonylhydroperoxide. This reaction mechanism yielded reactivity profile B in Figure 15. (** indicates that all of the sensitivity values were negligible.)

This leads us to conclude that, when *similar* activation barriers are used for the two isomerization routes, although the O_2QOOH isomerization to carbonylhydroperoxide is favorable or at least comparable to the alternative isomerization path, the products formed via the alternative O_2QOOH isomerization route decompose more readily to OH and contribute to the increased reactivity observed in our mechanism, especially at higher temperatures. The fact that this feature is notable at higher temperatures conforms to the fact that the activation energy barriers associated with certain reactions are more easily overcome at higher temperatures.

Finally, we performed a simulation identical to that conducted for Figure 6, and as before, we assumed a homogeneous adiabatic reactor at TDC and used SENKIN[43] constant-volume simulations. For this simulation, we developed a version of our current (more reactive) mechanism that had all of these alternative O_2QOOH species and reactions removed, in order to investigate the effect of not considering O_2QOOH alternative reaction class at all. As for Figure 6, we used an average pressure of 8 atm, a diluent of N_2 only, and compressed-gas temperatures within the range of 650−900 K as the initial conditions for the
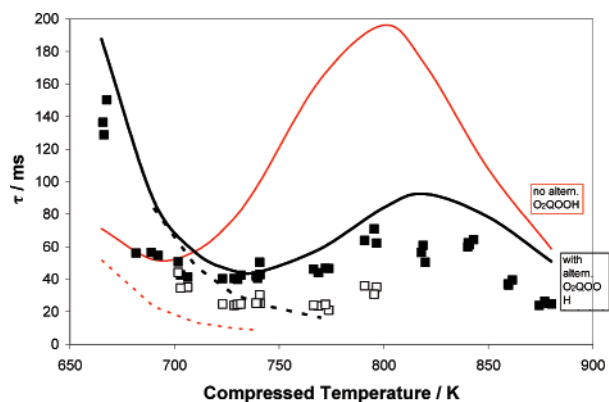
Figure 18. Experimental (points) ignition delay times for the pressure range of 7−9 atm and model-predicted values (lines) at 8 atm. The black line is for the version of the mechanism containing alternative O_2QOOH pathways, the red line is for the version of the mechanism without these species and reactions. Open symbols and dashed lines correspond to cool flame delay times.

constant-volume calculations. The results of the model-predicted ignition delay times excluding the alternative O_2QOOH reaction class are compared to the simulation in which such alternatives were included in the mechanism (at the same activation barrier as the O_2QOOH isomerization to carbonylhydroperoxide) in Figure 18.

Figure 18 shows that, in the low-temperature region of ∼665 K, the predicted ignition delay time was comparable to the experimentally recorded time. However, from 725 to 800 K, a large decrease in reactivity was seen for the version of the mechanism in which the alternative O_2QOOH reaction class was excluded. The reactivity of the mechanism deteriorated dramatically, such that peak of the NTC region was at ∼190 ms in comparison to ∼90 ms for the mechanism in which alternative O_2QOOH was included. In addition, the peak of the NTC was slightly offset, occurring at ∼800 K in comparison to the slightly higher temperature of ∼820 K for both the model in which alternative O_2QOOH was included and the experimental data. We conclude from these calculations, showing a high sensitivity in relation to the alternative O_2QOOH pathways, that the inclusion of such alternative O_2QOOH isomerizations, forming new O_2QOOH rather than the conventional isomerization route to carbonylhydroperoxide and hydroxyl radical, when the activation energy used is comparable to that of the reaction of O_2QOOH forming carbonylhydroperoxide, is important for the accurate prediction of ignition delay times for cyclohexane and accounts for much of the reactivity of the system in the temperature range of 700−850 K.

Inclusion of Heat Loss and the Compression Stroke. In experiments involving rapid compression machines, the issue of heat loss to the combustion chamber as well as the reaction occurring during the compression stroke is frequently discussed.[27,48−50] Indeed, heat loss is commonly neglected in simulations, and very often, reactions can occur in the final portion of the compression stroke that are likely to contribute to fuel consumption, especially when ignition delay times are quite short, such as those observed for *n*-heptane in rapid compression machine studies.[48,51] Lemaire et al.[11] reported that, for the Lille RCM cyclohexane studies, reaction during the compression stroke was never detected under their experimental conditions, because no traces of oxidation products were recorded at TDC.

We developed a heat loss profile for the Lille rapid compression machine, in an effort to better characterize our reactive simulations of oxidation in this machine. The effect of heat loss to the combustion chamber walls was estimated by matching
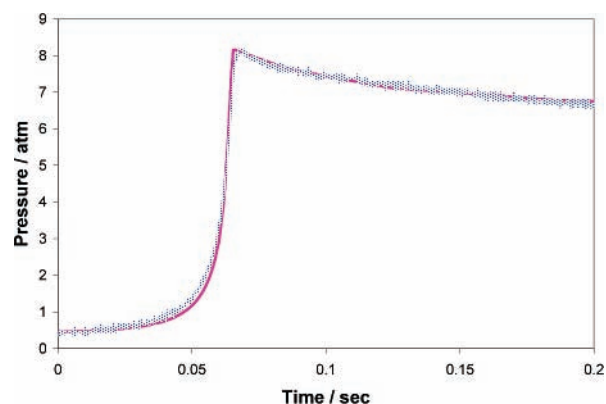

Figure 19. Experimental pressure−time data from an RCM (blue lines) and pressure−time profile obtained using the volume history generated in this work (solid magenta line). Mixture conditions as defined for mixture 4 in Table 4, using an unreactive mechanism (no reactions), initial pressure p_i = 350 Torr, initial temperature T_i = 351 K, experimental core gas temperature T_c = 737 K, and predicted core gas temperature T_c = 736.5 K.

TABLE 4: Mixture Compositions Used for Volume History Optimization

mixture	CHX	O_2	CO_2	N_2	Ar
1	0.0228	0.2053	0.1775	0.5944	0
2	0.0228	0.2053	0.0772	0.6947	0
3	0.0228	0.2053	0	0.7719	0
4	0.0228	0.2053	0	0.6175	0.1544
5	0.0228	0.2053	0	0.5403	0.2316
6	0.0228	0.2053	0	0.386	0.3856
7	0.0228	0.2053	0	0.2756	0.4963
8	0.0228	0.2053	0	0.193	0.5789
9	0.0228	0.2053	0	0.1158	0.6561
10	0.0228	0.2053	0	0.054	0.7179
11	0.0228	0.2053	0	0	0.7719

experimental and computed pressure histories for nonreactive gas mixtures. The volume history for the compression stroke was based on a displacement history provided by the Lille group. The displacement history was slightly modified to achieve the experimentally measured pressure at the end of compression. After the end of compression, the volume was expanded to simulate the effect of heat loss, which reduces the pressure and thus the temperature in the chamber. The adiabatic core gases that control autoignition are mainly affected by heat loss in this manner. This approach follows that of Tanaka et al.[52] and Mittal et al.[53] The resulting computed pressure history incorporating the compression stroke and postcompression period is shown in Figure 19 and is compared to the experimentally measured pressure history.

Experimentally measured pressure histories for nonreactive mixtures (where O_2 is replaced by N_2) corresponding to the reactive mixture compositions in Table 4 were provided by the Lille RCM group, and these were used to establish the accuracy of the volume history generated in our study.

In addition, we tested our accuracy in predicting the compressed-gas pressure using the reactive experimental mixture compositions in Table 4, with the O_2 component included, but using a mechanism in which all of the reaction rate constants are set to 0. The comparison of the experimental compressed-gas temperature and the simulated compressed-gas temperature is illustrated in Figure 20.

In a series of calculations, we examined the effects of including different degrees of fidelity in the compression and heat-transfer model. We compared three cases at a compressed-gas temperature of approximately 737 K: (1) a constant-volume

Chemical Kinetic Modeling of Cyclohexane Oxidation

J. Phys. Chem. A, Vol. 111, No. 19, 2007 **3771**

TABLE 5: Effects on Simulated Ignition Delay Time of Problem Type and Inclusion or Exclusion of a Heat Loss Profile

problem type	T_c (K)	τ (ms)	cool flame (ms)
1. adiabatic	737	37	27
2. postcompression + Q	737	41	33
3. full stroke + Q	735.5	40	32
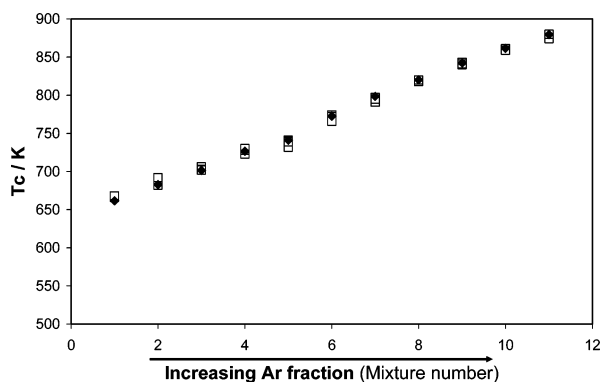
Figure 20. Compressed-gas temperature predicted using the volume history profile generated in this work (solid symbols) versus experimental compressed-gas temperature (open symbols). The mixture composition is according to Table 4. The model is the version using a mechanism in which no reactions are allowed. For both model and experiment, initial temperature $T_i = 354$ K and initial pressure $p_i = 350$ Torr.

Figure 21. Experimental (points) ignition delay times for the pressure range of 7−9 atm and predicted values for the model including heat loss (lines). Open symbols and dashed line correspond to cool flame delay times.

calculation with no heat loss, (2) the postcompression period only with heat loss, and (3) the full compression stroke and postcompression period with heat loss included throughout.

Mixture composition 4 (Table 4) was used, and the results of the different calculations are reported in Table 5:

The largest change in the results is seen from case 1, in which the heat loss after compression was neglected, to case 2, in which the heat loss is included (Table 5). Very little difference was noted between case 2, in which the compression stroke was not considered, and case 3, in which the full compression stroke was included. This reinforces the conclusion of Lemaire et al. that reaction during the stroke is not an important consideration at this compressed-gas temperature, for cyclohexane experiments in the Lille RCM.[11]

The reactive model with our heat loss profile and with full simulation of the compression stroke was used to compute ignition delay times in the RCM over the entire range of temperatures (Figure 21). Inclusion of the heat loss profile and the full compression stroke led to an increase of approximately a factor of 7 in computer time. The initial mixture compositions are defined in Table 4, and the initial temperature and pressure for each were 354 K and 350 Torr, respectively. The elongation of the predicted ignition delay time in the temperature range of 650−700 K, compared to that of the adiabatic, constant-volume simulation illustrated in Figure 6, is due to the inclusion of a heat loss model. As temperatures of 725 K and greater are reached and the NTC region is encountered, the model prediction with heat loss actually simulates the experimental data slightly better than the adiabatic calculation because cooling of the mixture causes it to react faster in the NTC region. At the higher temperatures of 860−870 K, the temperatures during the compression stroke are high enough to induce reactions, and the ignition delay times are marginally shorter than those from an adiabatic constant-volume calculation.

Jet-Stirred Reactor Experiments. Voisin et al.[12] and El Bakali et al.[13] reported experimental results on the oxidation of cyclohexane in a jet-stirred reactor incorporating the low- and
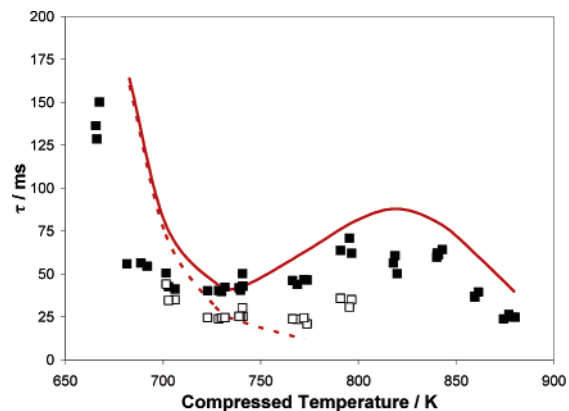
high-temperature regimes (750−1150 K), with equivalence ratios of $0.5 \leq \varphi \leq 1.5$; at 99% dilution by nitrogen; and at pressures of 1, 2, 5, and 10 atm. The residence times were 0.07 s for 1 atm, 0.1 s for 2 atm, 0.25 s for 5 atm, and 0.5 s for 10 atm. Low-temperature chemistry characteristics were not observed experimentally. Under the very dilute conditions of these experiments, the concentrations of cyclohexyl radical and O_2 are very low, so that little of the cyclohexylperoxy (RO_2) radical that is needed for low-temperature chemistry is formed.

Simulations were performed under isothermal, constant-pressure conditions assuming perfect mixing of the reactants. Reactant, intermediate product, and final product concentrations were obtained and are compared to the experimental results in Figures 22−26. We first present the results at the lowest pressure considered (2 atm), for stoichiometric mixtures of 0.15% cyclohexane in Figure 22.

Overall, species concentrations are reproduced satisfactorily. Figure 22a shows the profiles for fuel, oxygen, carbon monoxide, and carbon dioxide, as well as hydrogen and formaldehyde. The predicted fuel consumption is somewhat faster than that obtained experimentally above 900 K, and thus, the subsequent predictions of the formation of various species are less accurate and deviate from the experimental profiles (Figure 22b,c). Note that the experimental fuel profile shows an extended flat region from 850 to 1050 K. The end of this extended flat region is the minimum temperature for reaction. The extended flat region is shortened at 10 atm as seen in Figures 24−26. At higher pressures, it is possible for the fuel mixture to react at lower temperatures.

For the next series of results, the pressure was increased to 5 atm, and the mixture was stoichiometric with 0.15% cyclohexane (Figure 23). The predicted species concentrations at this pressure are considerably better than those predicted at 2 atm, with the experimental profiles being produced quite well. Figure 23a shows that the profiles for fuel, oxygen, carbon monoxide, and carbon dioxide, as well as hydrogen and formaldehyde, are all predicted well by the model. Figure 23b presents profiles for methane, ethylene, and 1,3-butadiene, among other species. These are quite well predicted, although ethylene is somewhat underpredicted, especially at 960 K, where it peaks in the experimentally recorded profile. The reactions forming ethylene will be discussed later. Figure 23c shows that cyclohexene is well predicted, although the predicted model profile peaks at the slightly lower temperature of 850 K in contrast to the experimental peak at ∼875 K. Other species, including cyclohexa-1,3-diene and benzene, are overpredicted by the model.
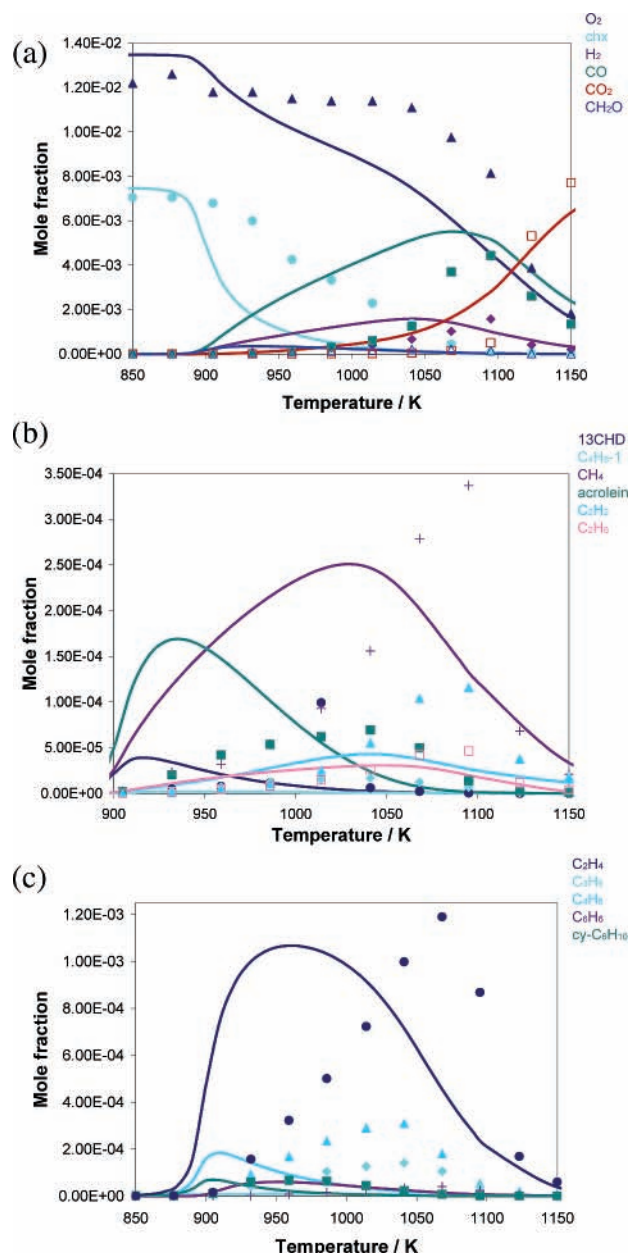
Figure 22. Cyclohexane oxidation at 2 atm (0.15%, $\varphi = 1.0$, $\tau = 0.1$ s) in a jet-stirred reactor. Experimental (points)[13] and model-predicted mole fractions for some of the species reported in the experimental study. Experimental and simulated fuel concentrations are shown increased by a factor of 5 for clarity.

Figure 23. Cyclohexane oxidation at 5 atm (0.15%, $\varphi = 1.0$, $\tau = 0.25$ s) in a jet-stirred reactor. Experimental (points)[54] and model-predicted mole fractions for some of the species recorded in the experimental study. Experimental and simulated fuel concentrations are shown increased by a factor of 5 for clarity.

Figure 24 shows comparisons between computed and experimental results for a stoichiometric mixture at the highest pressure considered (10 atm), with 0.1% cyclohexane and at a residence time of 0.5 s. The model performs well in predicting fuel consumption; oxygen depletion; and the formation of hydrogen, carbon monoxide, carbon dioxide, and formaldehyde (Figure 24a). In Figure 24b, the productions of methane and cyclohexene are particularly well captured. The model predicts less ethylene than observed in the experiments of Voisin et al.,[12] especially at temperatures such that the fuel has mostly been consumed. This discrepancy will be discussed later. In addition, benzene is overpredicted, as are buta-1,3-diene and cyclohexa-1,3-diene (Figure 24c).

Agreement was acceptable for most of the simulations. The effect of pressure on our model predictions is depicted in Figures 22–24, and we find that, at the lower pressure of 2 atm, our
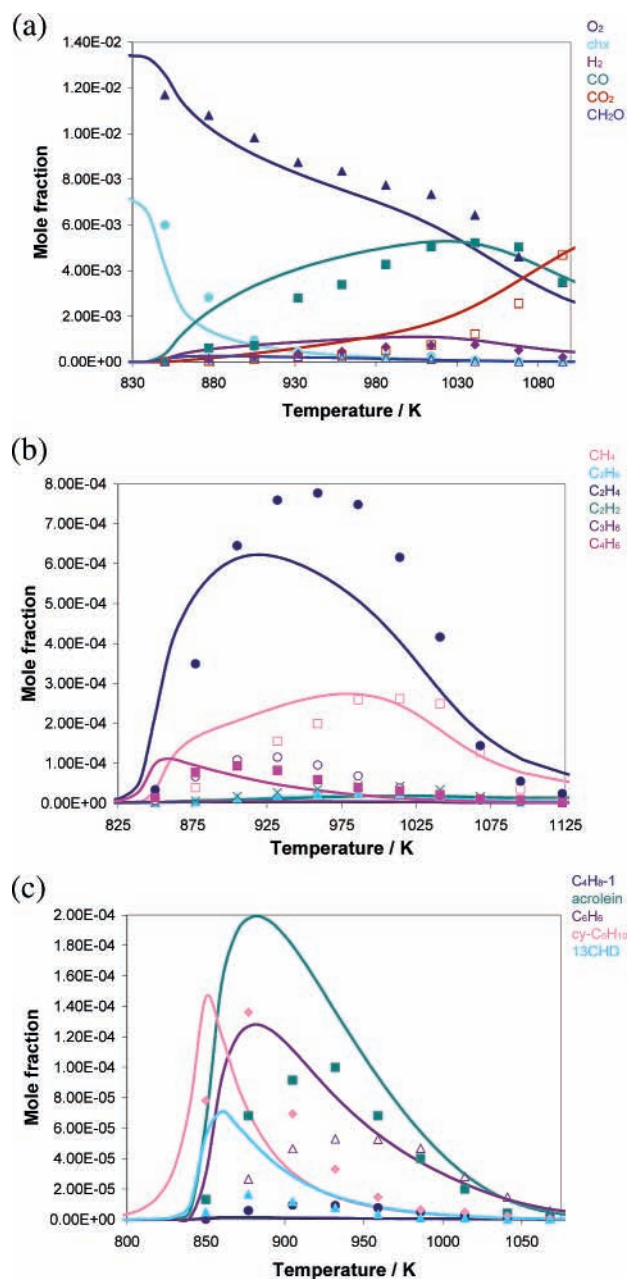
simulation is less accurate overall than our simulation at the higher pressure of 10 atm. It might be that our model does not accurately reflect the pressure dependence, and this warrants more attention and investigation.

In the earlier jet-stirred reactor work of Voisin et al.,[12] experimental data for cyclohexane at HCCI-like conditions of $\varphi = 0.5$ and $p = 10$ atm were reported. Figure 25 shows comparisons between computed and experimental results for these conditions. Overall, species concentrations are reproduced very well (Figure 25a–c). Most notably, our model is still ineffective at predicting ethylene in jet-stirred reactor environments. In addition, the model continues to overpredict cyclohexa-1,3-diene and benzene. The experimental measurements for these conditions are notable at temperatures greater than 750 K. An interesting feature is that our model predicts NTC-type
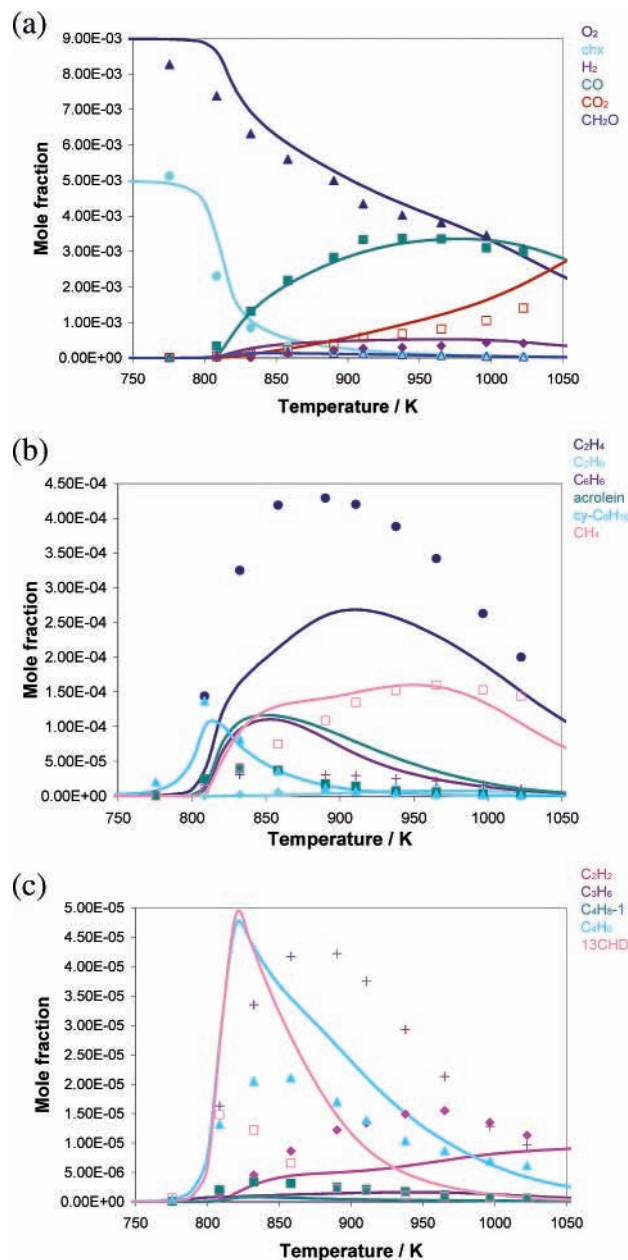
Chemical Kinetic Modeling of Cyclohexane Oxidation

J. Phys. Chem. A, Vol. 111, No. 19, 2007 **3773**

Figure 24. Cyclohexane oxidation at 10 atm (0.1%, $\varphi = 1.0$, $\tau = 0.5$ s) in a jet-stirred reactor. Experimental (points)[12,13] and model-predicted mole fractions for some of the species reported in both experimental studies. Experimental and simulated fuel concentrations are shown increased by a factor of 5 for clarity.

Figure 25. Cyclohexane oxidation at 10 atm (0.1%, $\varphi = 0.5$, $\tau = 0.5$ s) in a jet-stirred reactor. Experimental (points)[12] and model-predicted mole fractions for some of the species reported in the experimental studies. Experimental and simulated fuel concentrations are shown increased by a factor of 10 for clarity.

behavior in the temperature range of 700−800 K for ethylene (Figure 25b), buta-1,3-diene, cyclohexene, cyclohex-1,3-diene, and benzene (Figure 25c). This feature was not captured in the experiments, where data were recorded at temperatures of ∼750 K and greater and results at temperatures below 750 K were not reported.

In addition, Voisin et al. reported experimental data for cyclohexane at fuel-rich, diesel-like conditions of $\varphi = 1.5$ and $p = 10$ atm.[12] The model predicts a number of the species concentrations quite well (Figure 26a−c). The shape of the fuel profile is well captured by the model.

Ethylene continues to be underpredicted—a feature that this mechanism has repeatedly shown. At the lower simulated pressures of 2 and 5 atm, the model-predicted amount of ethylene was acceptable. However, at the higher pressure of 10
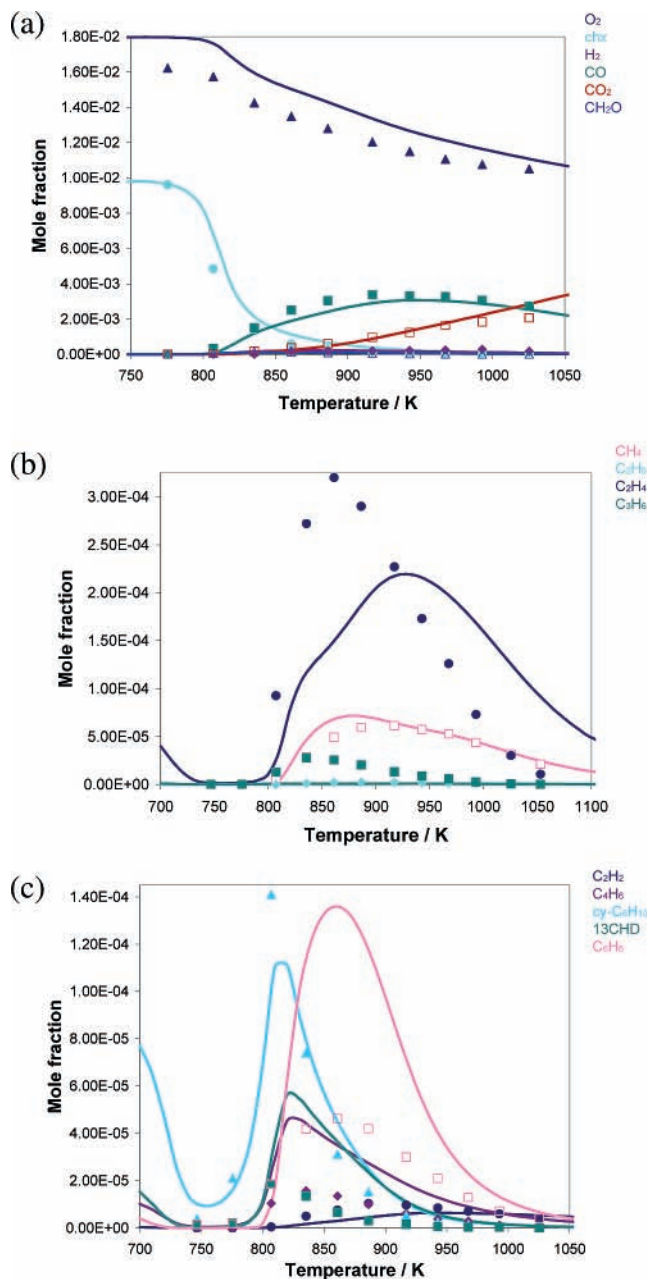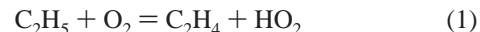
atm, the model faired less well in matching the experimental quantities of ethylene. An analysis of rate of production at approximately 900 K was carried out for each of the jet-stirred reactor conditions simulated in this work. Interestingly, for each of the conditions, 80% of the production of ethylene was from the same three reactions:

$$C_2H_5 + O_2 = C_2H_4 + HO_2 \qquad (1)$$

$$C_2H_4 + C_4H_7 1{-}4 = C_6H_{11}{-}16 \qquad (2)$$

$$C_4H_7 1{-}4 = C_2H_4 + C_2H_3 \qquad (3)$$

In reaction step 2 above, C_6H_{11}-16 is the olefinic radical produced from the ring-opening step of the fuel molecule. Figure
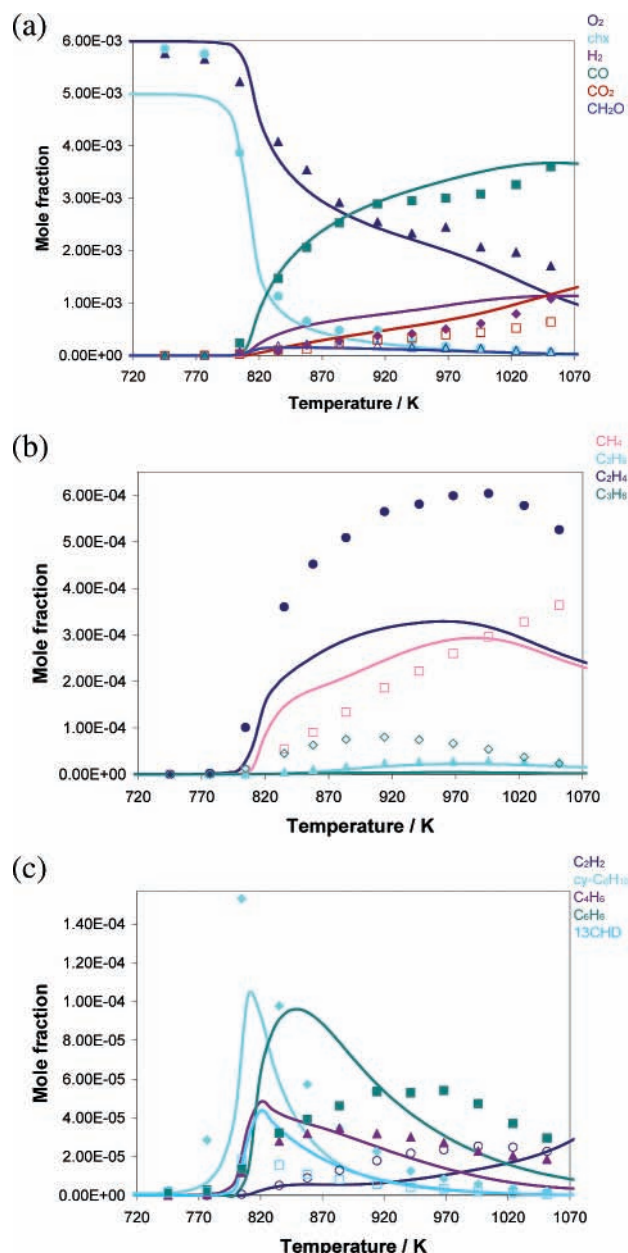
Figure 26. Cyclohexane oxidation at 10 atm (0.1%, $\varphi = 1.5$, $\tau = 0.5$ s) in a jet-stirred reactor. Experimental (points)[12] and model-predicted mole fractions for some of the species reported in the experimental studies. Experimental and simulated fuel concentrations are shown increased by a factor of 5 for clarity.

2 in the Chemical Kinetic Mechanism section of this article illustrates the formation of C_6H_{11}-16. The problem of simulating C_2H_4 concentrations needs further investigation.

Variation in the oxygen concentration at a constant pressure of 10 atm was found to change the overall reactivity of the system. Under conditions of high oxygen concentrations (1.8% O_2; Figure 25a–c), the fuel was oxidized at lower temperatures relative to stoichiometric conditions depicted in Figure 24a–c. Under conditions of low oxygen concentrations (0.6% O_2), oxidation occurred at higher temperatures relative to the stoichiometric experiments and simulations (Figure 26a–c).

Conclusions

The present study has developed a detailed reaction mechanism for the oxidation of cyclohexane. The mechanism was used to simulate cyclohexane oxidation in both a rapid compression machine and a jet-stirred reactor, incorporating the temperature range 650–1150 K, the pressure range of 1–12.5 atm, and various equivalence ratios. The overall reactivity of cyclohexane oxidation is well reproduced by the model, particularly for rapid compression machine experiments. In addition, many of the experimentally quantified intermediate species profiles from rapid compression machine studies are well reproduced by the model. This would indicate that most of the chemical pathways leading to the formation of such species are well understood. However, the model was not able to reproduce the experimentally observed amount of 1,2-epoxycyclohexane. This result indicates a potential problem in the current understanding of the R + O_2 reaction system. When the direct elimination of HO_2 from RO_2 is included, the formation of 1,2-epoxycyclohexane is unfavorable. Some attention is required to improve the model simulations of jet-stirred reactor experiments.

This mechanism was based on our previous modeling of hydrocarbon oxidation, particularly that of methylcyclohexane, as we attempted to confirm and extend the conclusions of that work in relation to specific rules for cyclic systems. In addition, our goal was to develop a unified approach to cycloalkanes such that similarities and differences in the correction terms between cyclic and acyclic isomerization reactions were determined. In this work, we establish a methodology for addressing cyclic hydrocarbon species that can be used in future mechanism development for other cyclic species.

An important feature of this mechanism is its ability to predict the formation of benzene via the dehydrogenation of cyclohexane. The benzene prediction under jet-stirred reactor conditions was quite good. However, improvement is needed for benzene prediction in rapid compression machine environments. Depending on the experimental conditions, reports in the literature state that the dehydrogenation of cyclohexane to produce benzene or routes that require aromatic ring formation by reactions involving C_3H_3, C_4H_5, and similar smaller species are the dominant pathways leading to soot formation. Under the conditions of the present study, we observed benzene formation from the dehydrogenation pathway.

Supporting Information Available: Chemical kinetic mechanism and thermochemical property files. This material is available free of charge via the Internet at http://pubs.acs.org.

References and Notes

(1) Walsh, C. *Canada's Oil Reserves 2nd Only To Saudi Arabia*. Available at http://www.rense.com/general37/petrol.htm; Dow Jones Newswire, petroleumworld.com, 5/6/2003.

(2) Westbrook, C. K. *Global Climate and Energy Project*; Stanford University, June 13–16, 2005; available at http://gcep.stanford.edu/pdfs/uQx8GXJG882-3q6NMuyQOw/westbrook_symp05.pdf.

(3) Guthrie, J.; Fowler, P.; Sabourin, R. *Gasoline and Diesel Fuel Survey*, Environment Canada: Gatineau, Quebec, Canada, 2003; available at http://www.ec.gc.ca/cleanair-airpur/CAOL/OGEB/fuels/reports/fullreport/pdf/FullReport2003_e.pdf.

(4) Law, M. E.; Westmoreland, P. R.; Cool, T. A.; Wang, J.; Hansen, N.; Taatjes, C. A.; Kasper, T. *Proc. Combust. Inst.* **2007**, *31*, 565.

Chemical Kinetic Modeling of Cyclohexane Oxidation

J. Phys. Chem. A, Vol. 111, No. 19, 2007 **3775**

(5) Gulati, S. K.; Walker, R. W. *J. Chem. Soc., Faraday Trans.* **1989**, *85*, 1799.

(6) Handford-Styring, S. M.; Walker, R. W. *Phys. Chem. Chem. Phys.* **2001**, *3*, 2043.

(7) Westbrook, C. K. *Proc. Combust. Inst.* **2000**, *28*, 1563.

(8) Simmie, J. M. *Prog. Energy Combust. Sci.* **2003**, *29*, 599.

(9) Sirjean, B.; Buda, F.; Hakka, H.; Glaude, P. A.; Fournet, R.; Warth, V.; Battin-Leclerc, F.; Ruiz-Lopez, M. *Proc. Combust. Inst.* **2007**, *31*, 277.

(10) Dayma, G.; Glaude, P. A.; Fournet, R.; Battin-Leclerc, F. *Int. J. Chem. Kinet.* **2003**, *35*, 273.

(11) Lemaire, O.; Ribaucour, M.; Carlier, M.; Minetti, R. *Combust. Flame* **2001**, *127*, 1971.

(12) Voisin, D.; Marchal, A.; Reuillon, M.; Boettner, J. C.; Cathonnet, M. *Combust. Sci. Technol.* **1998**, *138*, 137.

(13) El Bakali, A.; Braun-Unkhoff, M.; Dagaut, P.; Frank, P.; Cathonnet, M. *Proc. Combust. Inst.* **2000**, *28*, 1631.

(14) Billaud, F.; Chaverot, P.; Berthelin, M.; Freund, E. *Ind. Eng. Chem. Res.* **1988**, *27*, 759.

(15) Bonner, B. H.; Tipper, C. F. H. *Combust. Flame* **1965**, *9*, 317.

(16) Zeelenberg, A. P.; de Bruijn, H. W. *Combust. Flame* **1965**, *9*, 281.

(17) Snee, T. J.; Griffiths, J. F. *Combust. Flame* **1989**, *75*, 381.

(18) Klaï, S. E.; Baronnet, F. *J. Chim. Phys.* **1993**, *90*, 1929.

(19) Klaï, S. E.; Baronnet, F. *J. Chim. Phys.* **1993**, *90*, 1951.

(20) Davis, S. G.; Law, C. K. *Combust. Sci. Technol.* **1998**, *140*, 427.

(21) McEnally, C. S.; Pfefferle, L. D *Combust. Flame* **2004**, *136*, 155.

(22) Buda, F.; Heyberger, B.; Fournet, R.; Glaude, P. A.; Warth, V.; Battin-Leclerc, F. *Energy Fuels* **2006**, *20*, 1450.

(23) Cavallotti, C.; Rota, R.; Faravelli, T.; Ranzi, E. *Proc. Combust. Inst.* **2007**, *31*, 201.

(24) Granata, S.; Faravelli, T.; Ranzi, E. *Combust. Flame* **2003**, *132*, 533.

(25) Miller, J. A.; Pilling, M. J.; Troe, J. *Proc. Combust. Inst.* **2005**, *30*, 43.

(26) Bennett, P. J.; Gregory, D.; Jackson, R. A. *Combust. Sci. Technol.* **1996**, *115*, 83.

(27) Curran, H. J.; Gaffuri, P.; Pitz, W. J.; Westbrook, C. K. *Combust. Flame* **1998**, *114*, 149.

(28) Curran, H. J.; Gaffuri, P.; Pitz, W. J.; Westbrook, C. K. *Combust. Flame* **2002**, *129*, 253.

(29) Pitz, W. J.; Naik, C. V.; Ní Mhaoldúin, T.; Westbrook, C. K.; Curran, H. J.; Orme, J. P.; Simmie, J. M. *Proc. Combust. Inst.* **2007**, *31*, 267.

(30) Pitz, W. J.; Seiser, R.; Bozzelli, J. W.; Seshadri, K.; Chen, C. J.; Costa, I. D.; Fournet, R.; Billaud, F.; Battin-Leclerc, F.; Westbrook, C. K. *Chemical Kinetic Study of Toluene Oxidation under Premixed and Non-premixed Conditions*; Report UCRL-CONF-201575; Lawrence Livermore National Laboratory: Livermore, CA, 2003.

(31) Ritter, E. R.; Bozzelli, J. W. *Int. J. Chem. Kinet.* **1991**, *23*, 767.

(32) Lay, T. H.; Bozzelli, J. W.; Dean, A. M.; Ritter, E. R. *J. Phys. Chem.* **1995**, *99*, 14514.

(33) Benson, S. W. *Thermochemical Kinetics*; John Wiley and Sons: New York, 1976.

(34) Orme, J. P.; Curran, H. J.; Simmie, J. M. *J. Phys. Chem. A* **2006**, *110*, 114.

(35) Tsang, W. *Int. J. Chem. Kinet.* **1978**, *10*, 1119.

(36) Scott, M.; Walker, R. W. *Combust. Flame* **2002**, *129*, 365.

(37) Curran, H. J. *Int. J. Chem. Kinet.* **2006**, *38*, 250.

(38) Matheu, D. M.; Green, W. H.; Grenda, J. M. *Int. J. Chem. Kinet.* **2003**, *35*, 95.

(39) Walker, R. W.; Morley, C. In *Comprehensive Chemical Kinetics*; Compton, R. G., Hancock, G., Eds.; Elsevier: New York, 1997; Vol. 35, p 1.

(40) DeSain, J. D.; Klippenstein, S. J.; Miller, J. A.; Taatjes, C. A. *J. Phys. Chem. A* **2003**, *107*, 4415.

(41) Carstensen, H.; Naik, C. V.; Dean, A. M. *J. Phys. Chem. A* **2005**, *109*, 2264.

(42) Tsang, W.; Hampson, R. F. *J. Phys. Chem. Ref. Data* **1986**, *15*.

(43) Kee, R. J.; Rupley, F. M.; Miller, J. A.; Coltrin, M. E.; Grcar, J. F.; Meeks, E.; Moffat, H. K.; Lutz, A. E.; Dixon-Lewis, G.; Smooke, M. D.; Warnatz, J.; Evans, G. H.; Larson, R. S.; Mitchell, R. E.; Petzold, L. R.; Reynolds, W. C.; Caracotsios, M.; Stewart, W. E.; Glarborg, P.; Wang, C.; Adigun, O.; Houf, W. G.; Chou, C. P.; Miller, S. F. *Chemkin Collection*, version 3.31; Reaction Design Inc.: San Diego, CA, 2001.

(44) Kee, R. J.; Rupley, F. M.; Miller, J. A.; Coltrin, M. E.; Grcar, J. F.; Meeks, E.; Moffat, H. K.; Lutz, A. E.; Dixon-Lewis, G.; Smooke, M. D.; Warnatz, J.; Evans, G. H.; Larson, R. S.; Mitchell, R. E.; Petzold, L. R.; Reynolds, W. C.; Caracotsios, M.; Stewart, W. E.; Glarborg, P.; Wang, C.; Adigun, O.; Houf, W. G.; Chou, C. P.; Miller, S. F.; Ho, P.; Young, D. J. *CHEMKIN*, release 4.0.2; Reaction Design, Inc.: San Diego, CA, 2005.

(45) Silke, E. J. The Influence of Fuel Structure as Demonstrated by the Isomers of Heptane: A Rapid Compression Machine & Detailed Kinetic Modeling of *n*-Heptane. Ph. D. Thesis, National University of Ireland, Galway, Ireland, 2005.

(46) Silke, E. J.; Curran, H. J.; Simmie, J. M. *A Rapid Compression Machine Modelling Study of the Heptane Isomers*; European Combustion Meeting: Louvain-la-Neuve, Belgium, Apr 3−6, 2005.

(47) Sun, H.; Bozzelli, J. W. *J. Phys. Chem. A* **2004**, *108*, 1694.

(48) Griffiths, J. F.; Halford-Maw, P. A.; Rose, D. J. *Combust. Flame* **1993**, *95*, 291.

(49) Griffiths, J. F.; Hughes, K. J.; Schreiber, M.; Poppe, C. *Combust. Flame* **1994**, *99*, 533.

(50) Cox, A.; Griffiths, J. F.; Mohammed, C.; Curran, H. J.; Pitz, W. J.; Westbrook, C. K. *Proc. Combust. Inst.* **1996**, *26*, 2685.

(51) Silke, E. J.; Curran, H. J.; Simmie, J. M. *Proc. Combust. Inst.* **2005**, *30*, 2639.

(52) Tanaka, S.; Ayala, F.; Keck, J. C. *Combust. Flame* **2003**, *133*, 467.

(53) Mittal, G.; Sung, C.-J. *Combust. Flame* **2006**, *145*, 160.

(54) El Bakali, A. Physicochimie des Processus de Combustion et de l'Atmosphere, UMR CNRS 8522, Universite des Sciences et Technologies de Lille. Private communication, 2006.